PROJECTIVE GEOGRAPHIC POSITION DETERMINATION FROM STAR PHOTOGRAPHY*†

Dr. C. A. Traenkle, Scientist in Aeronautical Research Laboratory, Wright Air Development Center, Wright Patterson Air Force Base

1. Statement of Problem and Review of Methods

THE well known interconnection between the position of the stars and the geographic position of any station on the surface of the earth has always been used to determine those geographical positions by star observations. In Figure 1, the geographic station G on the globe is projected by the gravity vertical OG into the Zenith Z on the celestial sphere. The geographic coordinates of G or Z are defined in the geographic coordinate system by the longitude angle λ_z between the reference meridian GR (Greenwich) and the local meridian and by the latitude angle φ_z between the equator and Z. The position of any star Q on the celestial sphere is given by the right ascension a_Q, the angle between the reference meridian Υ of the vernal equinox and the star meridian, and by the declination δ_Q, the angle between the equator and Q. The stars Q undergo an apparent diurnal rotation around the axis OP. For any moment, given in Greenwich Civil Time (GCT), the relative position of the two systems is determined by the known angle $Gr\Upsilon$ between the two reference points, the so called Greenwich Hour Angle of Υ (GHAΥ), which is tabulated in the astronomical ephemerides. If, by chance, a star could be observed just at the zenith, the geodetic coordinates of Z would be

$$\lambda_z = \text{GHA}\Upsilon - a_z, \qquad \phi_z = \delta_z. \tag{1}$$

As such a star is not normally available, one has to refer to a neighboring and identifiable star Q, whose position is observed and defined in the local horizontal coordinate system by the azimuth angle α and the angular zenith distance z. By means of these data, the celestial coordinates of Z can be hooked up to those of Q, as shown in any nautical[1] or geodetic[2] handbook. The geographic coordinates of Z are determined by Equation (1). There exist, of course, various modifications in measuring those angles α and z, e.g. by theodolites, sextants, astrolabes, as are described in these handbooks. A new approach for this problem is to photograph the star configuration surrounding Z, as introduced, for example, by the Air Force $XA-12''$—Zenith camera[3]; by this the coordinates α, z of a multitude of stars are simultaneously recorded. Then the final geographic coordinates of Z are computed by analytic reduction executed on the photographic coordinates of some identifiable stars. The same basic idea has also been applied in the MM 101 Surveying Camera by E. L. Merritt.[4]

The methods to be demonstrated in this paper exploit the potentialities of the zenith star photography: They use the projective properties of radial directions in the photograph; these bring the decisive advantage of being independent from lens distortion and atmospheric refraction; this gain is lost in using the other methods with zenith distances. By an optical mechanical adjustment of the radial triangulation, all the available stars can be put into opertion for error reduction and compensation. Additionally, the interior orientation

* The author acknowledges the encouragement given by Colonel L. B. Williams, Dr. J. E. Clemens, Mr. B. B. Johnstone, Aeronautical Research Laboratory and the assistance of Mr. H. Speer, Aerial Reconnaissance Laboratory, Wright Air Development Center.

† Release for publication given by USAF Technical Information and Intelligence Branch. WPAFB.

of the camera and further check conditions are determined by a circular reversal process of the photographs around the full angular circle. All these measures, rapidly consummating highly overdetermined data, result in a remarkably high accuracy even with non-metric cameras and open up new fields of mass application.

2. Azimuth Projection and Transformation of Star Constellations

2.1 Star photograph and gnomonic star projection

The stars can be considered as located on the celestial sphere of infinite radius (Figure 1). Before the exposure, the camera axis is set coincident with the gravity vertical by means of cross levels. Consequently, the photographic plane is parallel with the tangential plane Z, and the star images Q' projected by the rays OQ may be related immediately to the tangential plane Z; in this case the length OZ may be considered as the focal distance F of the photograph and Z as its principal point. The configuration of the star images on plane Z is a gnomonic or azimuthal projection of their configuration on the celestial sphere, and in interpreting it as a projection, the distance OZ may be also taken eventually as unit of length.

2.2 Radial chart, radial triangulation

On the other hand, those gnomonic star projections may be computed and constructed exactly to scale related to a unit distance $OZ = F$, resulting in a computed star chart. The coordinates $(a_C \delta_C)$ of its origin Z_C are arbitrarily chosen as rounded off values in the neighborhood of the photographically recorded station Z_P. Of special importance is the set of azimuthal or radial rays from the origin Z_C to the Q'_i, wherefore the setup is denoted as a "Radial Chart." The direction set of the radial rays is practically not altered by a transprojection into the plane Z_P according to the well known procedure of radial triangulation in photogrammetry.[5] As shown in Figure 2, this direction set of the radial chart Z_C is put into coincidence with the star images Q'_i of the photograph Z_P. This is most accurately and directly made on an enlarged projection of the photograph, for example as in a "Kodagraph"-projector. The procedure of the mechanical optical adjustment is very simple: Radials of approximately opposite direction (e.g. Q_1, Q_3) are slid through their correspond-

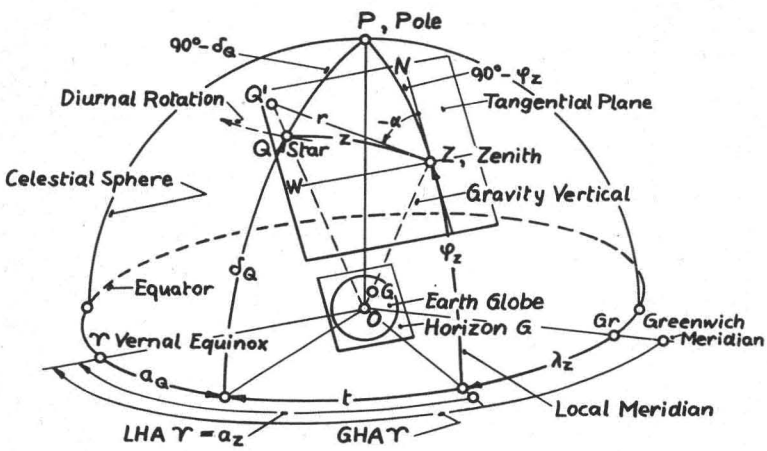

FIG. 1.—Geographic and Celestial Coordinates

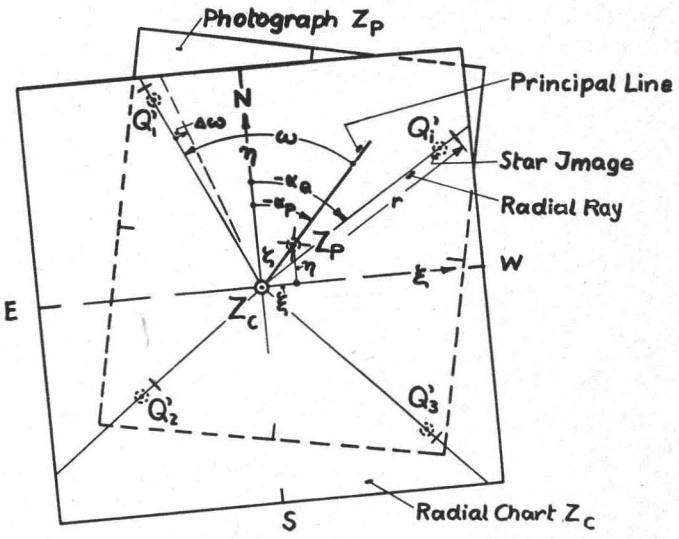

FIG. 2.—Gnomonic Projections, viewed from inside celestial sphere

ing photographic points until a cross radial (e.g. Q_2) hits its point. All the other overdetermined points should then fall automatically on their rays. Small deviations are meaned out, reducing and compensating efficiently the resultant error. After the adjustment of the chart, the coordinates of Z_P can be measured with reference to the ξ, η-coordinate system, for example by means of a scale edge (Figure 3), and these are finally converted into the increments of the geographic coordinates Z_P with reference to the known Z_C, as shown below.

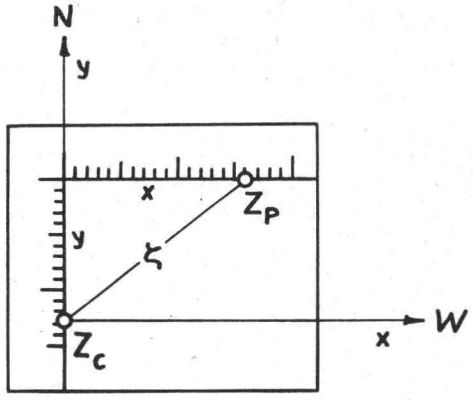

FIG. 3.—Scale Edge

The two projection planes Z_C and Z_P form the tilt angle ζ, represented in Figure 2 by the vector ζ lying in the principal line. The transprojection from the plane Z_C into Z_P slightly alters the directions ω of the radials by an amount $\Delta\omega$, which is small of second order, as can be easily deduced by simple geometry:

$$\Delta\omega = -\frac{\zeta^2}{4} \sin 2\omega.$$

Even if these corrections should be perceptible for individual rays, they cancel out for the over-all picture of the full angular circle by a changing of signs, and therefore, can always be disregarded.

The important advantage of the radial ray method is its insensitivity against lens distortion and atmospheric refraction. These radial displacements of the photograph are lying practically in the direction of the rays of the radial chart, as ξ, η are small quantities compared with the unit $OZ = F$. Their influence on

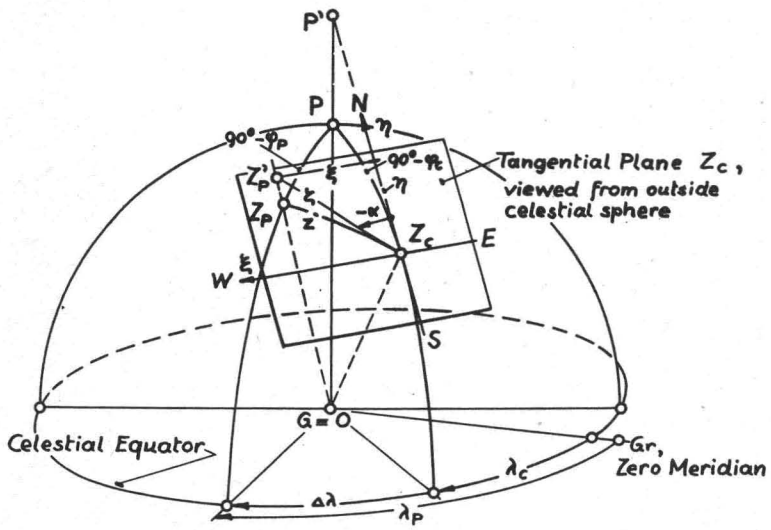

FIG. 4.—Coordinate Transformation

the adjustment process is therefore negligible and becomes even exactly zero for the limit $\xi, \eta \to 0$. In analogy to this radial chart method which uses only the azimuth angles of the star positions, there exists another method namely that of the position lines with equal altitude angles, according to Marc St. Hilaire,[1] where essentially the altitude angles of the star positions are used. This method is preferentially applied in navigation with sextants used as altitude measuring instruments. But here the radial displacements of the atmospheric refraction including the horizon depression (dip angle) must be very carefully accounted for. The uncertainties of these corrections, however, preclude the same high accuracy as by the radial chart method.

2.3 COMPUTATION AND CONSTRUCTION OF RADIAL CHARTS

The coordinates (a, z) of any star Q in the radial chart are deduced from its celestial coordinates (a, δ) ordinarily by the theorems of spherical trigonometry, applied to the astronomical triangle PQZ (Figure 1); Z is here interpreted as Z_C of the radial chart with the coordinates $a_C\varphi_C$. This coordinate transformation could be performed, for example, by means of the tables H.O.214 of the U. S. Hydrographic Office.[6] But on account of higher accuracy and a close error analysis, the basic formulae must be used. The hour angle t of Q is:

$$t = a_C - a_Q \tag{2}$$

where a_C, a_Q are the right ascensions of Z_C and Q respectively. The zenith distance z of Q is obtained by the cosine theorem

$$\cos z = \cos \phi \cos \delta \cos t + \sin \phi \sin \delta, \tag{3}$$

the radial distance r is then

$$r = F \tan z, \tag{4}$$

related to the projective distance $OZ \equiv F$ of the chart, which is interpreted eventually as the focal distance of the enlarged projected star photograph.

The azimuth α comes at first by the sine theorem

$$\sin \alpha = \sin t \cos \delta / \sin z.$$

But as this formula becomes unreliable for $\alpha \rightarrow 90°$, the value of $\cos \alpha$, as derived by the cosine theorem, is also taken into account:

$$\cos \alpha = (\sin \delta - \sin \phi \cos z) / \cos \phi \sin z.$$

By eliminating $\sin z$:

$$\tan \alpha = (\cos \phi \cos \delta \sin t)/(\sin \delta - \sin \phi \cos z) \equiv A/B, \tag{5}$$

where

$$A = \cos \phi \cos \delta \sin t, \qquad B = \sin \delta - \sin \phi \cos z. \tag{5'}$$

For $A > B$, one uses

$$\cot \alpha = B/A. \tag{5''}$$

These formulae are evaluated in tabular form, as in Table 2 of Section 6. Thereafter the radial chart (see Figure 14) is constructed preferably on a sheet of transparent and non shrinkable film and to the scale of the focal distance F of the enlarged projected star photograph. The azimuthal directions (α) are plotted by cartesian or polar coordinatographs,[7] using $\tan \alpha$ or α respectively as the case may be. The radials should be engraved on the sheet as fine lines. The images Q' on the radials, together with the star names and magnitudes, are also marked, but only to help in identification. The adjustment process outlined in Section 2.2, works very rapidly. After having correlated, say three of the most distinct stars, all of the other ones fit quite by themselves: there is no identification problem.

2.4 COORDINATE TRANSFORMATION

The problem is now to deduce the geographic coordinates λ_P, ϕ_P of Z_P from the known coordinates λ_C, ϕ_C of Z_C by means of the components ξ, η of the increment vector ζ, measured in the radial chart. The geographic coordinates of Z_C follow from Equation (1) by substituting values for Z_C for values for Z.

$$\lambda_c = \text{GHA}\Upsilon - a_c, \qquad \phi_c = \delta_c, \tag{1'}$$

where a_C, δ_C are the celestial coordinates of Z_C of the radial chart. The GHA Υ depends on the exact timing of the exposures. The corresponding computations are compiled in tabular form as in Table 3. Originally the two gnomonic projections Z_C and Z_P of Figure 2 were conceived as being transprojected to Plane Z_P. But as this relationship is strictly reciprocal, it is reversed here (Plane Z_P transprojected into Z_C) to simplify the further analysis (see Figure 4). The vector ζ is hereby not changed, being in both cases

$$\zeta = \tan z, \quad \text{with} \quad \xi = \zeta \sin \alpha, \qquad \eta = \zeta \cos \alpha, \tag{6}$$

where the length units are GZ_P and GZ_C alternately, which also are interpreted as the focal distance F of the enlarged photo plane; it is therefore

$$\xi \equiv x_{CP}/F, \qquad \eta \equiv y_{CP}/F, \tag{6'}$$

where x_{CP}, y_{CP} are the components of the distance $Z_C Z_P$ in the photo plane-radial chart.

The exact solution results from the astronomical triangle PZ_CZ_P similar to the deductions of Section 2.3:

$$\left.\begin{aligned} \sin \phi_P &= \sin \phi_C \cos z + \cos \phi_C \sin z \cos \alpha \\ \sin \Delta\lambda &= \sin \alpha \sin z / \cos \phi_P \end{aligned}\right\}. \tag{7}$$

The increments of λ, ϕ are defined as:

$$\Delta\lambda = \lambda_P - \lambda_C, \qquad \Delta\phi = \phi_P - \phi_C, \tag{8}$$

from which

$$\lambda_P = \lambda_C + \Delta\lambda, \qquad \phi_P = \phi_C + \Delta\phi. \tag{8'}$$

Since $\Delta\lambda$, $\Delta\phi$ as well as ζ, ξ, η are small quantities, Equations (7) are expediently developed into series:

$$\Delta\lambda = \xi / \cos \phi_C, \qquad \Delta\phi = \eta \qquad \text{(1. order)}, \tag{9}$$

$$\Delta\lambda = \xi(1 + \tan \phi_C \eta)/\cos \phi_C, \quad \Delta\phi = \eta - \tan \phi_C \, \xi^2/2 \quad \text{(2. order)}, \tag{10}$$

which prove to be satisfactory approximations in most practical cases. These computations, resulting in the coordinates $\lambda_P \phi_P$, should be tabulated, for example, as in Table 4.

The relative adjustment of star photograph and radial chart determines not only the geographic coordinates of the camera station, but also the azimuthal orientation of the photograph with reference to the geographic meridian. Therefore, if a frame axis or side of the camera is pointed to some outstanding landmark by means of a diopter, its azimuth angle to true north can be determined directly; thus, such a station fulfills the prerequisites of a so-called La Place point.—Another application would be to orient the frame axis in the direction of a magnetic needle, thus determining the magnetic declination directly.

3. Circular Exposure Reversal for Interior Orientation

3.1 multiple photography

To this point it has been supposed that Z_P is the principal point of the photograph, i.e. the intersection of the vertical through the internal lens node with the horizontal photo plane. However, this restriction can be discarded by the known expediency of reversing two exposures azimuthally by 180 degrees, while keeping the camera leveled; this is also used by the zenith cameras, quoted in references 3 and 4. Now this device can be considerably extended and refined by arranging the reversals around the whole angular circle, not just for one diameter, thus resulting in considerable gain of accuracy and additional checks for correct operation.

An efficient arrangement for circular reversal is, for example, one with four exposure turns separated by 90 degrees each, eventually pointed after the four points of the compass. This disposition is shown in Figure 5. There are four systems of star trails superimposed in the same photograph. They are arranged around the common plumb point Z_0, i.e. the intersection of the gravity vertical through the internal lens node with the photographic plane. It is even admissible that the gravity vertical is not exactly perpendicular to the photo plane, but deviates therefrom by small tilt angles, as follows additionally from the transprojection quality of radial triangulation, expounded in Section 2.2. The four systems of stars are discriminated from one another by coding the star trails

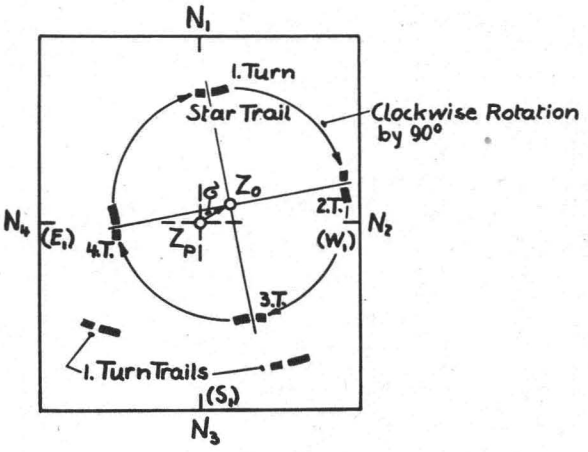

FIG. 5.—Multiple Star Photography

with a short and long exposure interrupted by a short break. These are made as short as possible, depending on the focal distance, only to give a still clearly discernible gap. The timing, preferably on the full minute, is laid in the middle of the break, as this point is most sharply defined. It is possible to cut down the time interval between two turns to one or two minutes, including the operations of exposure, turning and releveling.

3.2 POSITION REDUCTION AND COMPENSATION

The plumb point Z_0 defines the true local zenith and therewith, the true geographic coordinates of the station. It is separated from an available reference point Z_P, say the frame center, by a vector σ yet to be determined. Now in a first step, the geographic coordinates of the reference points Z_{P1} to Z_{P4} of the four turns are determined according to the procedures and formulae of Section 2. Their resulting positions are then plotted in a $\xi\eta$ coordinate system (see Figure 6). Obviously, they must be arranged regularly around Z_0: upon two rectangular diameters of a circle with Z_0 as center; i.e. the vector σ is rotated by 90 degrees for each turn. By this, there follows Z_0 as the center of the Z_{Pi} array, and as an additional operational check that the sequence of points Z_{Pi} has to form a regu-

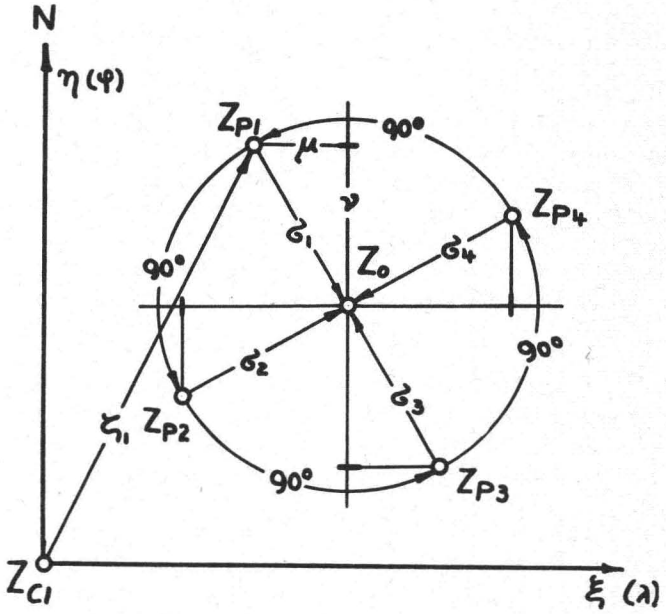

FIG. 6.—Position Reduction by Circular Reversal

lar square, as in Figure 7a. If this condition is not fulfilled, as in Figure 7b, the leveling operation has not been performed properly by the operator, and the photograph has to be rejected.

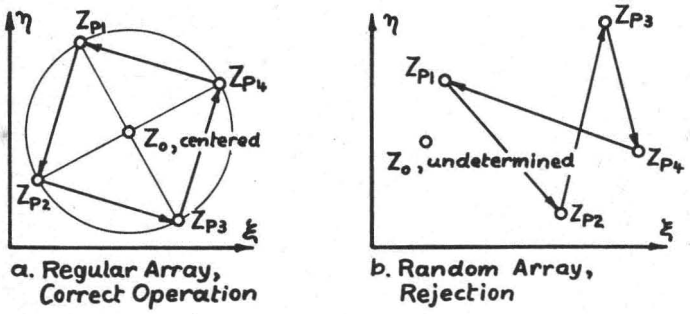

FIG. 7.—Operation Check

The configuration of the Z_{Pi} in Figure 6 could be used for a graphical compensation of the mean position Z_0. But as all the numerical data are compiled in tabular form, an analytic process is more convenient. The coordinates of Z_0 are the arithmetic mean of those of the Z_{Pi}

$$\lambda_0 = \sum_{i=1}^{4} \lambda_{Pi}, \qquad \phi_0 = \sum_{i=1}^{4} \phi_{Pi}. \tag{11}$$

To compute the components of vector σ there are first the components $\Delta\lambda\Delta\phi$ of the separation $Z_{Pi}Z_0$

$$\Delta\lambda_i^{(P0)} = \lambda_0 - \lambda_{Pi}, \qquad \Delta\phi_i^{(P0)} = \phi_0 - \phi_{Pi}, \tag{12}$$

wherefrom by means of Equation (9):

$$\sigma_{xi} = \Delta\lambda_i^{(P0)} \cos\phi_0, \qquad \sigma_{yi} = \Delta\phi_i^{(P0)}; \tag{13}$$

the "1. order" formulae (9) are here sufficient because σ will always be a very small quantity. In Figure 6 there can be seen how the components μ, ν of σ_1 reappear cyclically at the other turns. These interconnections can visually be reconstructed also in the tabular form of Figure 8: the μ and ν components are lying upon the broken μ and ν lines respectively, representing the cyclical periodic alternation; the signs are conserved when the lines are going to the direction of the principal, and reversed when in the direction of the auxiliary diagonal. The mean values of μ, ν are

$$\mu_0 = \frac{1}{m} \sum_{i=1}^{m} |\mu_i|, \qquad \nu_0 = \frac{1}{m} \sum_{i=1}^{m} |\nu_i|, \qquad m = 4, \tag{14}$$

which lead to the particular deviations

$$\Delta\mu_i = \mu_i - \mu_0, \qquad \Delta\nu_i = \nu_i - \nu_0; \tag{15}$$

by considering the error propagation, the RMS-error $\Delta\sigma$ follows

$$\Delta\sigma = \left[\sum_{i=1}^{m} (\Delta\mu^2 + \Delta\nu^2)/m - 1 \right]^{1/2}. \tag{16}$$

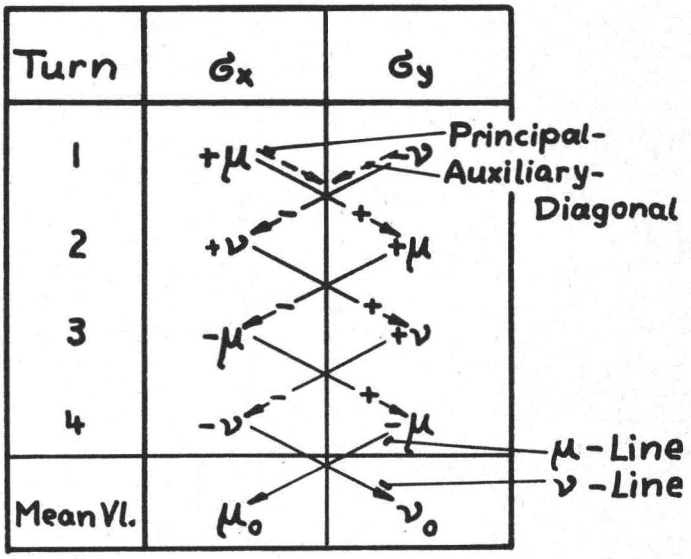

FIG. 8.—Analytic Compensation of σ-Components

Finally the mean coordinate errors result in

$$\epsilon_\lambda = \Delta\sigma/\sqrt{m}\cos\phi, \qquad \epsilon_\phi = \Delta\sigma/\sqrt{m}. \tag{17}$$

The numerical data according to these formulae are complemented in Table 4.

4. LENS DISTORTION, ATMOSPHERIC REFRACTION, CAMERA CALIBRATION

Although the effect of lens distortion has only negligible influence on the results, and although the missing interior orientation can be eliminated according to Sections 2.2 and 3 respectively, nevertheless, it might be of interest for test purposes to determine these data of camera calibration for nonmetric cameras. These measurements can be made after the field work at any later and more convenient time, by a simple and improvised laboratory set up. Such a calibration range simply consists of a pair of crossed scale strips nailed to the ceiling of a sufficiently high room, as shown in Figure 9. The star camera is positioned on the floor beneath the scale cross by means of a plumb line and is leveled by its own levels. The exposures are made with the lens stopped down. The photographs are immediately evaluated in an enlarging projector, e.g., a Kodagraph projector, in order to measure the lengths a' directly and conveniently. Therefore, all camera constants are re-

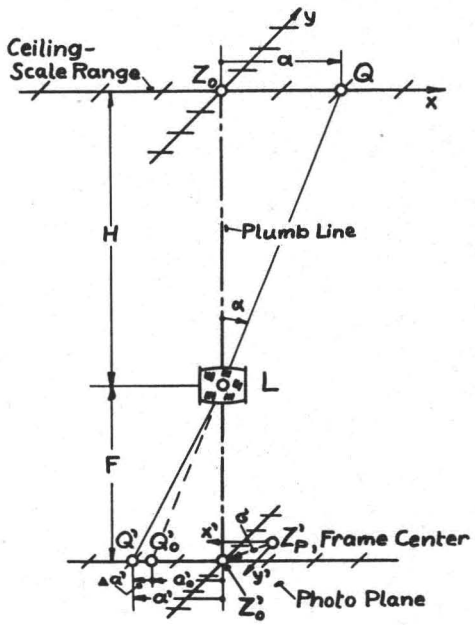

FIG. 9.—Calibration Range

ferred to the enlarged focal distance

$$F = kf, \tag{18}$$

where k is the magnification and f is the focal distance of the original camera. The undisturbed image position Q_0' is displaced by the distortion $\Delta a'$ into the actual position Q' with the coordinate a'. It is by definition[8]:

Equivalent focal distance

$$F_0 = H \left.\frac{a'}{a}\right|_{a \to 0},$$

Undistorted position

$$a_0' = a \frac{F_0}{H},$$

Distortion

$$\Delta a' = a' - a_0'.$$

Distortion curves of different lenses used for this project are compiled in Figure 10 as functions of the enlarged photographic coordinates a' on the projector screen. The curves are the totals of the camera and projector distortion together. The latter has been isolated in the diagram, and it can be seen that the camera

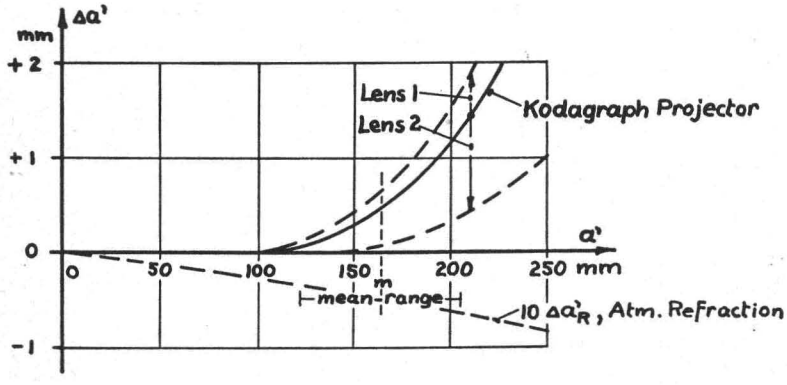

FIG. 10.—Distortion Curves

lens 2 is especially favorable as it partially compensates the projector distortion (reversed sign). By combining the appropriate lenses it is even possible to compensate the distortion perfectly, according to the Porro-Koppe principle. The best value of a mean focal distance F_m to use with the computations is that which corresponds to the mean working range of the a' coordinates

$$F_m = H \left.\frac{a'}{a}\right|_m = F_0 \left[1 + \left(\frac{\Delta a'}{a_0'}\right)_m\right], \tag{18'}$$

which is used in Equations 6 and 9 for the final coordinate increments $\Delta\lambda$, $\Delta\phi$. As these are already small quantities, obviously the error influence of F_m, as affected by uncompensated residual distortion, is small and of higher order, in accordance with the statement in Section 2.2 above.

The atmospheric refraction can be interpreted as an additional lens distortion, because the camera axis is pointed to the zenith, around which the atmos-

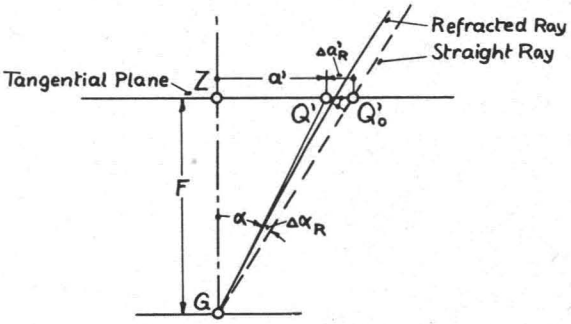

FIG. 11.—Atmospheric Refraction

pheric refraction is symmetrical. The refraction angle $\Delta\alpha_R$ according to astronomical handbooks is:

$$\Delta\alpha_R = -\epsilon \tan \alpha, \qquad (19)$$

where α zenith distance and $\epsilon = 1' = 1/3448$ rd. for the standard ground values of the atmosphere. The star image is displaced by $-\Delta\alpha_R'$ from Q_0' to Q' towards Z, according to Figure 11; the distortion is therefore negative. It follows from the geometry of Figure 11 and by substitution of Equation (19)

$$\Delta a_R' = F\Delta\alpha_R/\cos^2 \alpha = -F\epsilon \tan \alpha/\cos^2 \alpha. \qquad (20)$$

This function has been plotted in Figure 10 and can be composed with the other $\Delta a'$ to the resultant distortion magnitude. But its numerical influence is negligibly small, as can be seen from the graph.

The tilt components t of the photo plane with the vertical can be deduced from the left and right projections a_l' and a_r' of the sections $Z_0Q_l = -a$, $Z_0Q_r = +a$ according to projective relations,[9]

$$t \approx (-)2(a_l' - a_r')F/(a_l' + a_r')^2. \qquad (21)$$

As stated in Section 2 this deviation is very insensitive; it would be even tolerable if it keeps within such limits as to give at least still sharp imaging within the whole photographic fields.

Before the exposure, the point of the plumb line is accurately centered above the center of the front lens. Therefore Z_0' is the image of the true zenith Z_0 and the vector σ of the interior orientation is directly represented by its components $\sigma_x\sigma_y$ for example. The results are in good accord with those found by the star measurements of the numerical example of Section 6, Table 4.

The above calibration analysis and supplementary laboratory tests are confirmation that the measuring principles to be applied here are sound and insensitive to secondary disturbing influences.

5. Error Analysis

The objective is to deduce from the error Δr_Q of the photographic position of the stars as primary error source, the resulting error Δr_z of the geographical position, determined by the restitution process of Sections 2 and 3, and further to analyze the influence of complementary error sources. The methods used here are those developed in analogous projective problems.[10]

5.1 Resulting Error

The physical accuracy limit of the evaluation procedure is primarily determined by the position error $\Delta r_Q'$ of the photographic star images, due to lens aberrations and emulsion deficiencies. It has to be reduced first to the common datum of the projector screen and radial chart, in accordance with Equation (18).

$$\Delta r_Q = \frac{F}{f}\Delta r_Q', \qquad (22)$$

where the projector magnification is $k \equiv F/f$. The maximum error of Z_C in the adjustment of the radial chart by the minimum number of control points is now according to Figure 12

$$\Delta r_{Z\,mx} = \Delta r_Q,$$

while the RMS error Δr_z follows from the over determination of the data

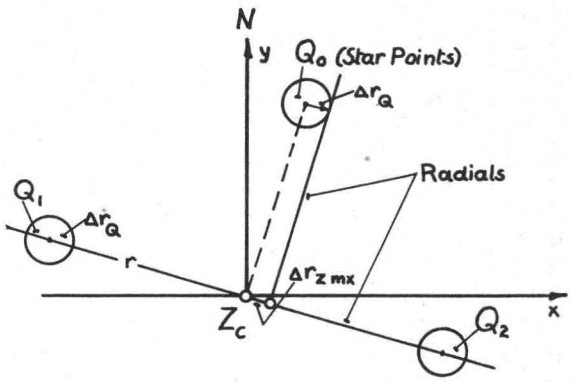

FIG. 12.—Error of Chart Adjustment

$$\Delta r_z = \Delta r_Q/\sqrt{N}, \qquad N = (n-3)m, \qquad (22')$$

where $(n-3)$ is the number of overdetermined radials, and m is the number of circular reversal turns. By substituting in Equation 9, the coordinate errors are finally

$$\epsilon_Z \equiv \Delta r_Z/F, \qquad \epsilon_\lambda = \epsilon_Z/\cos\phi, \qquad \epsilon_\phi = \epsilon_Z. \qquad (23)$$

The values of (23) are largely determined by the error Δr_Q which depends naturally on the focal distance and quality of the camera and projector, and whether the coincidence adjustment on the screen is made adequately by magnifying glasses and accurate glass scales (accuracy stage 1) or only by improvised means (accuracy stage 2). The numerical data, as related to the practical tests below and based on conservative estimates are compiled in Table 1. The remarkably high accuracy is due largely to the favorable error compensation formulated in Equation (22′)

5.2 COMPLEMENTARY ERROR INFLUENCES

Those errors enter the field during the subsequent stages of operation. The more important ones are: leveling and timing of the camera, construction of the radial chart, and measurement by the scale edge. Their respective errors Δr_T may be reduced also to the plane of the projection screen and radial chart. Those additional components should be held smaller than the primary error Δr_Q of Equation (22).

$$\Delta r_T < \Delta r_Q \quad \text{to} \quad \Delta r_T \ll \Delta r_Q. \qquad (24)$$

Position Errors	Δr_Q mm	ϵ_λ sec. of arc	$\epsilon_\varphi = \epsilon_Z$ sec. of arc
Accuracy Stage 1 (refined)	0.05	4.5″	3.5″
Accuracy Stage 2 (improvised eq.)	0.2	18	14

TABLE 1. THEORETICAL POSITION ERRORS OF Z. $n = 8$, $m = 4$, $N \approx 4.5$, $F \approx 620$ mm, $\varphi \approx 40°$

The resulting error is obtained by error propagation as an RMS value of the component terms, and in the case of Equation (24), the influence of those components compared to the primary error is negligible, constituting a kind of internal tuning.

Level Interval. The level can be set in a single setting to approximately $\frac{1}{4}$ of the level interval T_L, or better. The level error ϵ_L for $m=4$ reversals is therefore

$$\epsilon_L \approx T_L/4\sqrt{m} \approx T_L/8.$$

With the internal tuning condition $\epsilon_L < \epsilon_z$, there is for the level interval

$$T_L \lessapprox 8\epsilon_Z \tag{25}$$

and numerically

Accuracy Stage 1 $\quad T_L \approx 30''$ (sec. of arc),

Accuracy Stage 2 $\quad T_L \approx 2'$. (min. of arc).

These values are obtainable by ordinary commercial types.

Timing Error. The timing according to Section 3 is made by a break shutter. Even by a simple hand-operated flip flop type, it is possible to synchronize the break with a precision watch up to $\Delta t = \frac{1}{5}$ sec. This causes a longitude error

$$\Delta\lambda_t = 15\Delta t/\sqrt{m} = 1.5'' \text{ (sec of arc)}, \tag{26}$$

which is sufficiently small even for a higher accuracy stage.

Chart Error. This influence consists of a computational and a constructional phase. While the latter relates to the plotting of the star positions by means of a coordinatograph for which the accuracy can be easily held under control, the former requires a detailed analysis. The star position r, α is computed by Equations (3), (4), (5), and the objective is to determine its radial and tangential computation error $\Delta r_C^{(r)}$, $\Delta r_C^{(\alpha)}$ (see Figure 13), if the tabulated trigonometric functions entering the above equations have an inherent error e, of half a unit of the last digit.

Radial Component $\Delta r_C^{(r)}$. By differentiation of Equation (4):

$$\Delta r_C^{(r)} = F\Delta z/\cos^2 z \approx F\Delta z, \qquad \text{where } \cos z \approx 1 \text{ is a mean value.}$$

By differentiating Equation (3) and by summing the various terms quadratically for error propagation, the mean value Δz_m becomes

$$\Delta z_m \approx 5.6e$$

where

$$\Delta\cos\phi, \quad \Delta\cos\delta, \quad \Delta\cos t, \quad \Delta\sin\phi, \quad \Delta\sin\delta = e,$$

$$\phi_m, \delta_m \approx 45°, \quad Z_m \approx 0.265\text{rd}.$$

are mean values for the mean computation range; the rather high numerical factor 5.6 is indicative of the unavoidable error deterioration in the chain of formulae and computation. By substitution

$$\Delta r_C^{(r)} = 5.6Fe \tag{27}$$

and with the numerical values $F=620$ mm., $e=\frac{1}{2}10^{-4}$ (4 digit table)

$$\Delta r_C^{(r)} \approx 0.2 \text{ mm.},$$

which is sufficiently small in view of this radial error component not affecting the accuracy of the radial chart method.

Azimuthal Components $\Delta r_C^{(\alpha)}$. From the geometry of Figure 13 it is

$$\Delta r_C^{(\alpha)} = r\Delta\alpha.$$

The error $\Delta\alpha$ has to be derived from Equation (5) by differentiation

$$\Delta \tan\alpha = \left(\Delta A(+)\frac{A}{B}\Delta B\right)/B,$$

where $(+)$ is the symbol for the RMS summation and ΔA, ΔB have to be reduced by further differentiation to the error e finally. It results for the mean computation range

$$\Delta\alpha \approx 6e,$$

and by substitution

$$\Delta r_C^{(\alpha)} = 6r_m e; \tag{28}$$

this gives numerically with a 4 digit table $r_m \approx 165$ mm. (Figure 10).

$$\Delta r_C^{(\alpha)} \approx 0.05 \text{ mm.},$$

which is sufficient even for the accuracy stage 1.

Thus it is proven that the computation of the chart can be made satisfactorily accurate by means of 4 digit tables. It is not difficult to raise the computational chart accuracy by using higher digit tables. But this would not make sense unless all the other error influences are tuned up to such a higher standard.

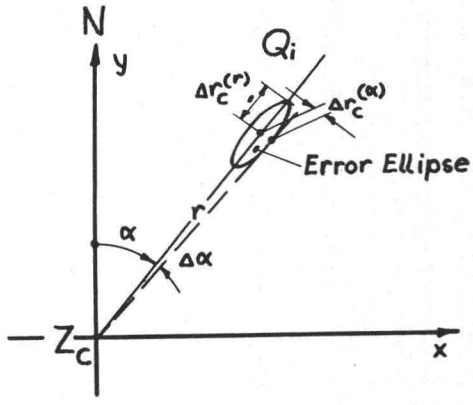

FIG. 13.—Chart Error of Stars

Coordinate Measurement by Scale Edge. After having adjusted the radial chart to the n radial points Q_i the coordinates of Z_P referred to Z_C, have to be measured by means of the scale edge. Its error Δr_{SC} obviously should be adapted to the Δr_Q of Table 1, taking into account the position Z_P being already determined within a reduced error by compensation of the overdetermined radials $(n-3)$:

$$\Delta r_{SC} \lessapprox \Delta r_Q/\sqrt{n-3} \approx \Delta r_Q/2, \tag{29}$$

and numerically

Accuracy Stage 1 $\Delta r_{SC} = 0.03$ mm.,
Accuracy Stage 2 $\Delta_{SC} = 0.1$ mm.

It follows that for Stage 2, ordinary scales are still sufficient, but that for Stage 1, glass scales and reading microscopes should be used.

6. Numerical Example

The above described new methods were tested by practical field operation. The star photography was made according to the technique of Section 3 by improvised adaptation of simple non-metric cameras. The first step in determining

Star[11] Name	Magn.	α			t	sin t	cos t	δ				sin δ	cos δ	cos z	r	A	B	tan α
		h	m	s	°			°	′	″	d°				mm			
335 ι Urs. Mj.	3.1	8	56	7.8	−14.033	.2425	.9702	48	13	25	.224	.7458	.6662	.9745	143.22	−.1238	+.1194	−1.0369
358 Θ Urs. Mj.	3.3	9	29	51.6	−22.465	.3821	.9241	51	53	15	.888	.7868	.6172	.9427	219.92	−.1807	+.1808	−0.9994
307 27 Lync.	4.9	8	05	39	− 1.266	.0221	.9997	51	38	34	.643	.7842	.6206	.9793	128.30	−.0105	+.1547	−0.067
292 24 Lync.	5.0	7	39	11.4	+ 5.202	.0907	.9959	58	49	23	.823	.8556	.5177	.9449	215.26	+.0360	+.2482	+0.145
280 19 Lync.	5.6	7	19	10.7	+10.205	.1772	.9842	55	22	23	.373	.8229	.5682	.9573	187.66	+.0771	+.2075	+0.371
1190 1281 Lync.	5.6	7	12	28.5	+11.881	.2059	.9785	47	19	34	.326	.7352	.6778	.9806	124.07	+.1069	+.1049	+1.019

TABLE 2. RADIAL CHART COMPUTATION. Chart 1: $a_c = 120°\ (8^h)$, $\varphi_c = 40°\ N$ } 3−21−54, $F = 621.6$ mm

Origin Data	Turn	Zone Time (45°W)			Watch Corr., Zone Corr.			GCT A^h			GHA ♈ [12] 0^h		Increm. [13] f. A^h		GHA ♈ A^h		Long. λ_c		
		h	m	s	h	m	s	h	m	s	°	′	°	′	°	′	°	′	d°
Chart 1	1	20	35	0	0	0	+19.6	23	35	19.6	177	58.6	354	48.0	172	46.6	52	46.6	.777
$a_c = 120°\ (8^h)$	2	20	37	0	+3	0	0	23	37	19.6			355	18.1	173	16.7	53	16.7	.278
$\varphi_c = 40°\ N$	3	20	39	0				23	39	19.6			355	48.2	173	46.8	53	46.8	.780
Date 3-21-54	4	20	41	0				23	41	19.6			356	18.3	174	16.9	54	16.9	.282

TABLE 3. CHART ORIGIN COORDINATES

Turn	x_P mm $\xi°$	y_P mm $\eta°$	$\lambda_c°$ $\Delta\lambda$	$\varphi_c°$ $\Delta\varphi$	$\lambda_P°$ λ_{P0}	$\varphi_P°$ φ_{P0}	$\sigma_x°$	$\sigma_y°$	Mean Values	x-Comp. °	y-Comp. °
1	+9.7 +0.894	−1.0 −0.092	+52.777 + 1.167	+40.000 − 0.092	+53.944 + 0.175	+39.908 − 0.180	+ 0.134	− 0.180	Mean Pos. Z_0 λ_0 φ_0	+54.119	+39.728
2	+ 5.1 +0.470	− 4.5 −0.415	53.278 +0.614	40.000 −0.415	+53.892 +0.227	+39.585 + 0.143	+0.174	+ 0.143	Vector σ μ_0 ν_0	.137	.179
3	+4.2 +0.387	−4.9 −0.452	+53.780 +0.505	+40.000 −0.452	+54.285 − 0.166	+39.548 + 0.180	−0.127	+0.180	Error $\Delta\sigma$ $\Delta\sigma^2$ $\Delta\sigma$	60 10^{-6}	$\pm 7.7\ 10^{-3}$
4	+0.6 +0.055	−1.4 −0.129	+54.282 + 0.072	+40.000 − 0.129	+54.354 − 0.235	+39.871 − 0.143	−0.180	−0.143	Error Z_0 ε_λ ε_φ	±0.005 ± 18″	±0.004 ±14″

TABLE 4. POSITION REDUCTION AND COMPENSATION

the geographic coordinates of the station G is to compute the radial chart for a point Z_C, with rounded off coordinates, roughly in the neighborhood of G, whereby the position of G has to be estimated first, at least roughly. But as angular differences up to 15 degrees can be tolerated, this makes no difficulty. The computations are made in accordance with Equations (2) to (5), and are compiled in Table 2, which is self-explanatory. The star coordinates can be taken from any star catalogue[11]. The computations are made by means of a desk computer and trigonometric four digit tables which can easily be handled and interpolated, especially in using decimals of angular degree. Therefore, in computing the hour angles from the right ascensions, this conversion is immediately made by the desk computer using the relations—

$$1 \text{ min. of time} = 0.016,\ 667 \text{ hour},$$
$$1 \text{ sec. of time} = 0.000,\ 278 \text{ hour},$$
$$1 \text{ hour} = 15°$$

The number of digits just safeguards the 0.001 degree angular unit on which the computations are based. For the conversion of direct angular measure, e.g. the declination angle, there is analogously

$$1 \text{ min. of arc} = 0.016,\ 67° \text{ (decimal of degree)},$$
$$1 \text{ sec. of arc} = 0.000,\ 28°$$

With the values tan α and r tabulated, the chart can be constructed (see Figure 14), the marked star magnitudes and zenith distances are helpful in identifying and correlating the radials for the coincidence adjustment. It is good practice to make a first rough draft of such a chart, supplemented by the hour meridians and declination circles, to have a first survey of the distribution of the available stars over its field.

In the next step the geographic coordinates of Z_C have to be fixed acc. to Equation (1′) for the time moments of the four exposure turns. The data are tabulated in Table 3. After the coincidence adjustment of the chart, the coordi-

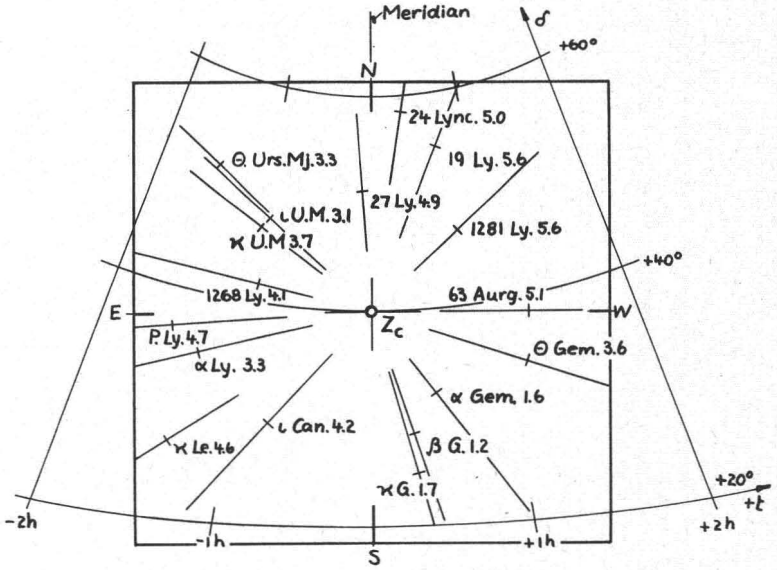

FIG. 14.—Sketch of Chart 1

nates of $Z_P(x_P y_P)$ can be measured with reference to Z_C and from that the geographic coordinates $Z_P(\lambda_P \phi_P)$ are deducible according to the formulae of Section 2.4 and as tabulated in Table 4. The latter is supplemented by the compensation process, executed on the four turns according to the formulae of Section 3.2, resulting finally in the mean coordinate errors $\epsilon_\lambda \epsilon_\phi$, experimentally determined. Comparing with Table 1, they are in close accord with the theoretical errors, Stage 2. Regarding the makeshift equipment which was available for the tests, the achieved accuracy is remarkably high going to the credit of the error compensating computation procedures. By slight and inexpensive refinements, as suggested in this paper, it would therefore be possible to attain accuracy stage 1 safely.

7. Standard Chart System

A distinct advantage of the radial chart procedure is that the charts can be prepared in advance to accelerate the evaluation. This could be made for large areas, whole latitude zones, or even the whole sphere, by relatively modest means: if the intervals of a_C and δ_C are made approximately 15 degrees, the whole sphere could be covered by approximately 200 charts.

Moreover, the charts, once available, can be used repeatedly over a long period of time, since the relative configuration of the stars is practically constant. Only the location of the celestial equatorial coordinate system undergoes slow changes by the precession of the vernal equinox and the nutation of the celestial pole. They influence only the coordinates of the chart origin $Z_C(a_C \delta_C)$ and the azimuth (α_N) of the meridian; they can be compensated, including the aberration effect, by the corrections:

$$\left.\begin{aligned} \Delta a_C &= F_1(a_C, \delta_C, t) \\ \Delta \delta_C &= F_2(a_C, \delta_C, t) \\ \Delta \alpha_N &= F_3(a_C, \delta_C, t) \end{aligned}\right\},$$

as functions of the chart coordinates $a_C \delta_C$ and the time t. These formulae could be compiled numerically in astronomical ephemerides.

8. Summary

The new radial chart and circular reversal procedures of zenith star photography make possible determining the geographical coordinates of stations on the earth with a considerably high accuracy and computational speed, even by simple non-metric cameras and inexpensive equipment. The reason for this is the insensitivity of the above procedures to camera calibration and its high error compensating power.

In connecting with a precomputed standard chart system, large projects over continental areas could be handled efficiently, like

1. Determination of a network of astronomical base points for topographical and photogrammetric mapping.
2. Determination of the deflections of the vertical within such a field by connecting its network of base points (La Place points) by geodetic measurements, i.e. survey of the geoid and the gravitational anomalies.
3. Survey of the magnetic declination.

References

1. Dutton, B., "Navigation and Nautical Astronomy," U. S. Naval Institute, Annapolis, 1948.
2. Roelofs, R., "Astronomy Applied to Land Surveying," J. Ahrend & Zoon, Amsterdam 1950.

3. AF Report on the XA-2-12″ Zenith Camera, Buckley Field, Colorado, 1945.
4. Merritt, E. L., "Principles of Design and the Applications of the M M 101 Surveying Camera," PHOTOGRAMMETRIC ENGINEERING XIX (1953), 779.
5. Kelsh, H. T. "Radial Triangulation," MANUAL OF PHOTOGRAMMETRY, VIII, 1952.
6. H. O. 214, "Tables of Computed Altitude and Azimuth," U. S. Navy Department Hydrographic Office, Washington D. C. 1939.
7. W. Meyer zur Capellen, "Mathematische Instrumente," Akademische Verlagsgesellschaft, Leipzig, 1944.
8. For a detailed representation: Traenkle, C. A., "Resection in Space by Projective Transformation," PHOTOGRAMMETRIC ENGINEERING XX (1954), p. 149 et seq.
9. See ref. 8, p. 146.
10. See ref. 8, p. 155.
11. "Apparent Places of Fundamental Stars 1954," Lord Commissioners of the Admiralty, London 1953.
12. "Solar Ephemeris 1954," Keuffel and Esser Company, New York, Table 12.
13. See Ref. 12, Table 5.

MEASUREMENTS OF CROWN DIAMETER AND CROWN COVER AND THEIR ACCURACY FOR 1:12,000 PHOTOGRAPHS*

David P. Worley and H. Arthur Meyer, Asst. Professor and Professor of Forestry respectively, School of Forestry, The Pennsylvania State University

ABSTRACT

The standard error of individual crown diameter measurements made with either the shadow wedge or with a dot transparency is between 3 and 4 feet. The results obtained with a calibrated shadow wedge are free of systematic errors, while the use of the dot transparency may lead to systematic errors amounting to about 1 or 2 feet. Measurements of crown cover percentage made with a dot grid or a crown density scale are affected by highly significant systematic errors or interpreter's bias. The maximum of these systematic errors is between 5 and 10 per cent. The standard error of an individual measurement for a given interpreter is equal to 10 per cent. Measurements made with the dot grid method are somewhat more objective and subject to smaller systematic errors than the measurements based on comparisons with a crown density scale.

TIMBER stand volumes of upland oak forests in Pennsylvania have been successfully correlated with various expressions of tree height, relative crown cover and visible crown diameter, variables which can be conveniently measured on 1:12,000 aerial photographs. Of these three variables, only tree height can be precisely measured on the ground, allowing an objective determination of the systematic as well as the accidental errors of measurement.[5] The visible crown diameters of trees in mixed hardwood stands as measured on aerial photographs cannot be checked by ground measurements. Multiple stem trees, interlocking crowns, shadow variations, all contribute to wide discrepancies between visible crown diameters measured on photographs and actual crown diameters measured from the ground. Similarly, relative crown cover in these stands usually expressed as a percentage of complete crown coverage, cannot be directly related to any particular determination of crown cover made on the ground. For these reasons only the relative accuracy of such measurements can be investigated, namely the variation in the measurements made by a single observer and the variation in the measurements between observers. In other words, it is only possible to ascertain the relative consistency of photo measurements between and within different photo interpreters. The photo measurements used in this investigation were all made on 1:12,000, photographs taken with an 8¼

* Authorized for publication on Dec. 1, 1954 as paper no. 1927 in the Journal Series of the Pennsylvania Agricultural Experiment Station.